Tuning the Coupling of an Individual Magnetic Impurity to a Superconductor: Quantum Phase Transition and Transport

Laëtitia Farinacci, Gelavizh Ahmadi, Gaël Reecht, Michael Ruby, Nils Bogdanoff, Olof Peters, Benjamin W. Heinrich, Felix von Oppen, and Katharina J. Franke

Phys. Rev. Lett. **121**, 196803 — Published 9 November 2018

DOI: 10.1103/PhysRevLett.121.196803

Tuning the coupling of an individual magnetic impurity to a superconductor: quantum phase transition and transport

Laëtitia Farinacci,[1] Gelavizh Ahmadi,[1] Gaël Reecht,[1] Michael Ruby,[1] Nils Bogdanoff,[1]
Olof Peters,[1] Benjamin W. Heinrich,[1] Felix von Oppen,[2] and Katharina J. Franke[1]

[1] *Fachbereich Physik, Freie Universität Berlin, Arnimallee 14, 14195 Berlin, Germany*
[2] *Dahlem Center for Complex Quantum Systems and Fachbereich Physik, Freie Universität Berlin, 14195 Berlin, Germany*

(Dated: October 9, 2018)

The exchange scattering at magnetic adsorbates on superconductors gives rise to Yu-Shiba-Rusinov (YSR) bound states. Depending on the strength of the exchange coupling, the magnetic moment perturbs the Cooper pair condensate only weakly, resulting in a free-spin ground state, or binds a quasiparticle in its vicinity, leading to a (partially) screened spin state. Here, we use the flexibility of Fe-porphin (FeP) molecules adsorbed on a Pb(111) surface to reversibly and continuously tune between these distinct ground states. We find that the FeP moment is screened in the pristine adsorption state. Approaching the tip of a scanning tunneling microscope, we exert a sufficiently strong attractive force to tune the molecule through the quantum phase transition into the free-spin state. We ascertain and characterize the transition by investigating the transport processes as function of tip-molecule distance, exciting the YSR states by single-electron tunneling as well as (multiple) Andreev reflections.

The exchange coupling of magnetic impurities to a superconductor induces localized Yu-Shiba-Rusinov (YSR) bound states [1–3]. Even for single impurities, the superconducting ground state depends qualitatively on the strength of the exchange coupling J (Fig. 1a). For weak coupling, the bound subgap state remains unoccupied, the superconducting ground state fully paired, and the impurity spin free. At strong coupling, the bound state becomes occupied and the superconducting ground state involves an unpaired electron which (partially) screens the impurity spin [4–8]. The level crossing between these states at a critical coupling J_c, commonly referred to as quantum phase transition, is protected by fermion-parity conservation. As states of different fermion parity exchange roles at the transition, the level crossing is immediately reflected in the single-particle addition spectrum. A discontinuity in the corresponding spectral weights and an abrupt change in the screened impurity spin make this a first-order transition. When including effects of self-consistency, additional discontinuities are predicted in the bound state energy and the local order parameter [9–11].

Experimental probes of magnetic-impurity physics use quantum dots or magnetic adatoms. For quantum dots, the exchange coupling J can be controlled electrically. Superconductor (SC)–quantum dot (QD)–SC junctions provide indirect evidence for the quantum phase transition through a 0–π transition of the Josephson current [12–14]. More immediate spectroscopic evidence emerges from measurements on asymmetric SC–QD–normal metal (N) junctions [15–17]. Typically obtained in the Coulomb-blockade regime at mK temperatures, the spectra are dominated by Andreev reflections and are thus insensitive to the spectral weights of the (single-particle) addition spectrum.

In contrast, probing magnetic adatoms with scanning tunneling microscopy (STM) readily provides access to both, single-electron and Cooper-pair (Andreev) tunneling by controlling the tunnel gap and varying the junction conductance over several orders of magnitude [18]. In the regime of single-electron tunneling, STM experiments measure the single-particle addition spectrum and thus provide crucial information about the quantum phase transition. In particular, tunneling spectroscopy (STS) provides access to the asymmetry between electron- and hole-like YSR excitations [18–26] which changes abruptly at the transition.

STM experiments are thus particularly well suited to probe the first-order nature of the transition. However, earlier experiments [21, 27, 28] could only access a discrete set of exchange couplings J determined by the adatom's adsorption site. Here, we use the flexibility of a single molecule adsorbed on superconducting Pb(111) to modify the molecule's interaction with the surface and tune the system continuously through the quantum phase transition. The superconducting tip exerts a force on the molecule which can be approximated by a Lennard-Jones potential (Fig. 1b). With tip approach and hence growing junction conductance, the force is initially attractive, increasingly lifting the molecule from the surface. This modifies characteristic parameters of the junction and in particular reduces the exchange coupling [29–31]. (For a discussion of the influence of other parameters, see supplementary material [32].) As the tip approaches further, the force becomes repulsive and pushes the molecule back towards the surface. This reverses the trend of the exchange coupling which now increases again. When combined with detailed conductance measurements to resolve the different tunneling processes, this technique allows for an in-depth analysis of the quantum phase transition.

We use Fe(II)-porphin (FeP) molecules deposited on a clean Pb(111) surface from a powder of Fe(III)-porphin-

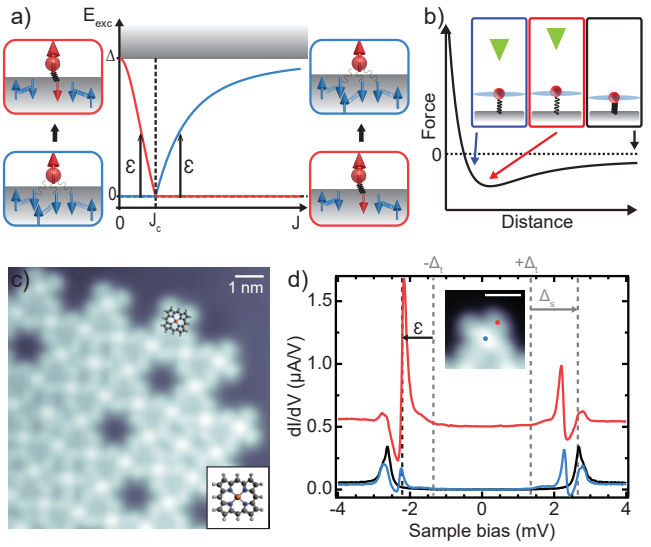

Figure 1. a) Schematic dependence of ground and excited states of a magnetic adatom on a superconducting substrate on exchange coupling strength J. At weak coupling, the ground state is a free-spin state, while the excited state has a quasiparticle bound to the adatom. At a critical coupling J_c, the roles of ground and excited states reverse. b) Sketch of the forces acting between tip and molecule vs. tip–molecule distance. At large distances, attractive forces pull the molecule away from the surface. At closer distance, repulsive forces push the molecule back towards the surface. c) STM topography image of a FeP island ($V = -45$ mV, $I = 50$ pA) with a molecular model (inset). d) dI/dV spectra acquired with a Pb tip above bare Pb(111) (black), center (blue) and ligand (red, offset for clarity) of a molecule.

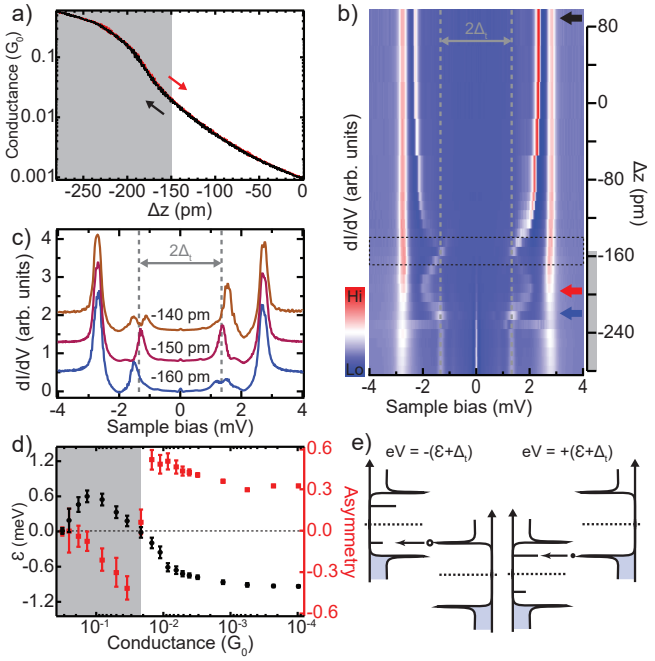

Figure 2. Tip approach above Fe center of a FeP molecule (for more data see [32]). a) Junction conductance (in $G_0 = 2e^2/h$) vs. tip offset Δz. b) 2D false-color plot of dI/dV spectra recorded at various tip-sample distances, normalized to their conductances at 5 mV. The spectra were acquired after opening the feedback at $V = 5$ mV, $I = 200$ pA and subsequently varying the tip height by an offset Δz (lock-in modulation $V_{\rm rms} = 15$ μV). c) Spectra before ($\Delta z = -140$ pm, brown trace), at ($\Delta z = -150$ pm, claret), and after ($\Delta z = -160$ pm, blue) the quantum phase transition (offset for clarity). d) Extracted YSR energies and intensity asymmetries vs. junction conductance. Error bars determined from peak widths and noise level of the spectra. Around $G = 0.02 \times G_0$ ($\Delta z = -150$ pm), the YSR state energy crosses zero and the asymmetry changes sign, indicating the quantum phase transition. e) Single-electron tunneling processes for YSR resonances at positive and negative bias voltages.

chloride (FeP-Cl). These molecules lose their Cl ligand by deposition below room temperature followed by annealing to 370 K (see [32]). STM experiments at a temperature of 1.6 K reveal the formation of well-ordered islands (Fig. 1c). The individual molecules are identified by their clover shape with a bright protrusion at the Fe center.

The superconducting Pb tips used to probe the YSR states of the molecule provide an effective energy resolution beyond the Fermi-Dirac limit. The measured signal is a convolution of the tip's Bardeen-Cooper-Schrieffer (BCS) density of states with the substrate density of states. Apart from peak intensity changes, the convolution shifts all spectral features of the substrate by the tip's superconducting energy gap Δ_t. The BCS peaks of the substrate are thus observed at bias voltages of $\pm(\Delta + \Delta_t)/e = \pm 2.65$ mV [33], where Δ denotes the gap of the substrate. Inside the gap, we find one pair of YSR states at ± 2.2 mV. These are resolved both on the Fe center and the ligand (Fig. 1d) so that both positions can be employed to investigate the tip-induced forces and the quantum phase transition.

We first characterize the junction conductance as the tip approaches the Fe center. We measure the tip approach Δz from a set point at $V = 5$ mV and $I = 200$ pA. As shown in Fig. 2a, the conductance first increases exponentially with Δz as expected for a tunnel junction. (Small deviations result from nonlinearities in the I-V converter at small current densities.) A super-exponential increase beyond $\Delta z = -150$ pm and subsequent leveling off indicate the transition to the contact regime between tip and molecule. Contact formation is fully reversible with identical approach and retraction curves, enabling precise tuning of the junction conductance.

As described above, the exchange coupling and hence the binding energy of the YSR states depend sensitively (but not monotonously) on the tip approach Δz. As the tip approaches the Fe center, we observe that the YSR states shift deeper into the superconducting gap

(Fig. 2b). At $\Delta z = -150$ pm, the YSR resonance occurs at a bias voltage equal to the tip's gap parameter, *i.e.*, at zero energy (see zoom in Fig. 2c). Approaching the tip further, the YSR states shift towards the superconducting gap edge before eventually reversing at $\Delta z = -190$ pm (red arrow in Fig. 2b) and reaching zero energy for a second time (blue arrow in Fig. 2b). This series of spectra thus follows the trend of initially decreasing and then increasing exchange coupling J, reflecting the force-distance curve in Fig. 1b. Beyond this point, at even closer tip–molecule distances, the spectra are dominated by peaks at zero bias and Δ_t.

Individual $\mathrm{d}I/\mathrm{d}V$ spectra do not allow for a complete identification of the binding energy of the YSR state since the same excitation energy may signify a screened or a free-spin ground state (see Fig. 1a). However, the observed shift of the YSR states deeper into the superconducting energy gap upon approach allows for an unambiguous assignment. As attractive tip–molecule forces initially lift the Fe center from the surface and weaken the exchange coupling J, the pristine system must be in the strong-coupling regime with a screened-spin ground state and a negative YSR energy.

We observe asymmetric intensities of the electron- and hole-like YSR resonances at positive and negative voltages, respectively. This asymmetry is a consequence of the potential scattering by the magnetic impurity. At large tip-molecule distances, the electron-like excitation has more spectral weight than the hole-like excitation. The relative strength changes with tip approach and accompanying YSR energy shift. In Fig. 2d, we plot the binding energy ϵ of the YSR state and the asymmetry $(I_+ - I_-)/(I_+ + I_-)$ as a function of junction conductance, with $I_{+/-}$ being the YSR intensities at positive and negative bias voltages, respectively. While the binding energy passes smoothly through zero, the zero-energy crossing coincides with an abrupt change in sign of the asymmetry.

These observations provide detailed evidence for a first-order quantum phase transition between screened-spin and free-spin ground states as the tip–molecule distance is reduced. For sufficiently weak tunneling, the current is dominated by single-electron tunneling (sketches in Fig. 2e) [18]. Hence, we can relate the observed intensities of the electron- and hole-like resonances to the local weights of the electron and hole wave functions of the YSR bound state (see [32] for additional details). Exciting the system out of the screened-spin YSR state annihilates a bound quasiparticle. For single-electron tunneling, this process involves $\gamma_0 = uc_\alpha - vc^\dagger_\beta$, where γ_0 (c_α) is the annihilation operator of the bound quasiparticle (electron with spin α). Correspondingly, the intensity of the electron-like excitation at positive bias voltages is given by $|v|^2$, as the bound electron combines with the tunneling electron to form a Cooper pair. Similarly, the hole-like excitation at negative bias is given by $|u|^2$, reflecting a bound electron tunneling out into the tip. The roles of u and v reverse when exciting the system out of the free-spin ground state and creating a bound quasiparticle, as described by $\gamma^\dagger_0 = u^* c^\dagger_\alpha - v^* c_\beta$. Now, electron tunneling at positive bias occupies the bound state and involves $|u|^2$, while tunneling at negative bias breaks a Cooper pair and involves $|v|^2$. The abrupt change in the asymmetry at a tip approach of $\Delta z = -150$ pm, where the YSR state crosses zero energy, is thus a hallmark of the first-order quantum phase transition. We also note that the gradual increase of the asymmetry before the quantum phase transition is in agreement with a decrease in the exchange coupling [9, 34].

Self-consistency causes additional discontinuities in the bound-state energy and the local order parameter near the impurity [9–11]. We do not find indications of these discontinuities. In [32], we derive analytical estimates for their magnitude. The discontinuity of the local gap parameter is substantial, of order $\delta\Delta \sim -\Delta/\ln(\omega_D/\Delta)$ within a few Fermi wavelengths of the impurity (ω_D is the Debye frequency), but cannot be directly probed by single-electron tunneling. The latter probes the bound state energy, whose jump is of order $\delta\epsilon \sim \Delta^2/[E_F \ln(\omega_D/\Delta)] \sim 10^{-2}$ μeV. This is orders of magnitude below our experimental resolution ~ 100 μeV. Instead of a discontinuity, we observe that the asymmetry vanishes right at the transition. This suggests that both $|u|^2$ and $|v|^2$ are probed simultaneously as is natural for a bound state whose energy vanishes within the resolution.

Next, we place the tip above the ligand. The $G - \Delta z$ curves exhibit the same stability and reversibility as on the center and allow for probing both the tunneling and the contact regime (Fig. 3a). At large tip-molecule distances, we find YSR states at the same bias voltages as above the Fe center, but with reversed asymmetry (Fig. 1d). The $\mathrm{d}I/\mathrm{d}V$ spectra at different junction conductances (Fig. 3b) also show the initial shift of the YSR states deeper into the superconducting energy gap. However, the YSR states do not reach or cross zero energy. The YSR states come closest to zero energy for $\Delta z = -150$ pm before shifting back to higher energies as a result of the molecule being pushed back towards the surface (Fig.1b). The measured asymmetry confirms that the system does not pass through the quantum phase transition (Fig. 3c). Indeed, the asymmetry does not change sign at $\Delta z = -150$ pm and the hole-like excitation remains stronger than the electron-like excitation throughout (see detailed spectra in Fig. 3d). A change in asymmetry occurs only upon further approach (Fig. 3c,d) when resonant Andreev reflections become the dominant tunneling process [18].

Importantly, the overall trend of the YSR shift resembles the case with the tip above the Fe center, reflecting an analogous dependence on the tip–molecule force. Hence, despite the inverse asymmetry, the YSR state re-

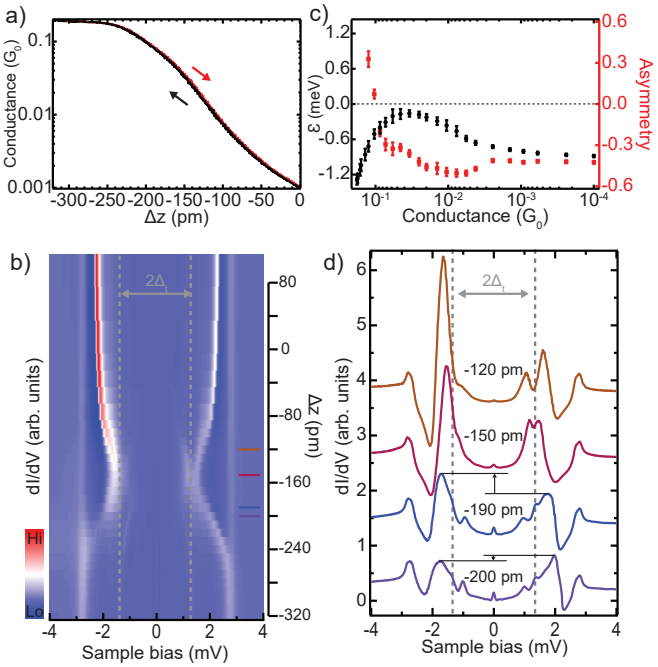

Figure 3. Tip approach above Fe ligand of FeP molecule (see Fig. 1b) (for more data see [32]). a) Evolution of conductance with tip offset Δz. b) 2D false-color plot of dI/dV spectra recorded at various tip-sample distances, normalized to their conductances at 5 mV. c) Extracted YSR energies and intensity asymmetries vs. junction conductance. d) Four spectra of this approach set (offset for clarity). The YSR state does not reach zero energy and the asymmetry remains positive during most of the approach, see the brown, claret, and blue spectra in panel d). The asymmetry reverses only around $G = 0.1 \times G_0$ where Andreev reflections become dominant, see blue and purple spectra in panel d.

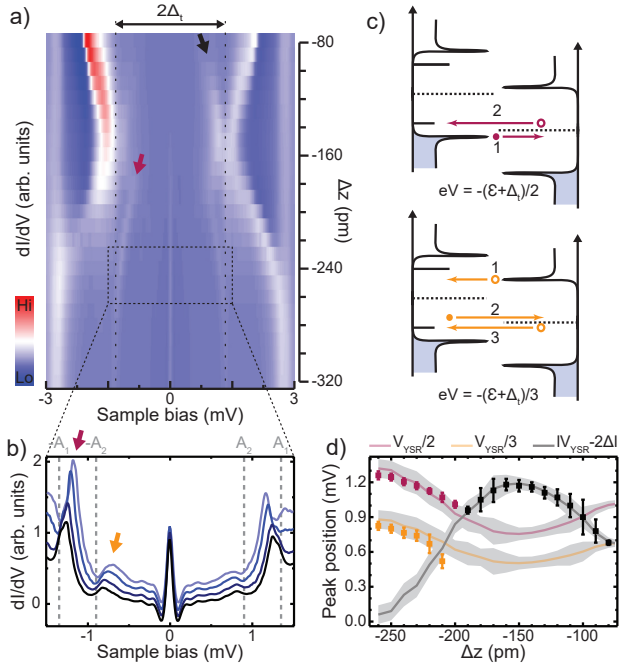

Figure 4. a) Closer view of the approach set in Fig. 3b. b) Four spectra (offset for clarity) of this set showing two peaks due to the Andreev processes depicted in c). An electron (hole) is reflected through the junction until its energy matches the YSR state. d) Extracted positions of the peaks shown in a and b (rectangles) as well as traces showing the expected positions of a thermal excitation of the YSR state (black trace) and of the processes shown in c (yellow and pink) given the position of the YSR state.

flects the same ground state. Given that we observe the same energy on ligand and center, we suggest that the YSR state arises from a delocalized spin state associated with Fe d_π states hybridized with π states of the ligand [35–37]. The absence of a quantum phase transition on the ligand reflects differences in the elastic response of the molecule to the applied force.

So far, we could understand all spectral features in terms of single-electron excitations of the YSR states. We already noted that on both Fe center and ligand, the asymmetry is reduced at tip approaches of $\Delta z \approx -190$ pm. The continuous change of spectral intensity can be explained by resonant Andreev reflections gaining strength as the tunnel conductance increases [18]. Furthermore, we observe the onset of a zero-bias resonance as a fingerprint of Cooper pair (Josephson) tunneling upon further increase of the junction conductance. (Refs. [31, 38] also observed Josephson peaks in STM spectra of single adatoms and molecules at close tip–sample distance.) In addition, we find peaks at $eV = \pm\Delta_t$. We interpret these as the threshold for the lowest-order ($n = 2$) multiple Andreev reflections (MAR), generally expected at $eV_n = \pm(\Delta + \Delta_t)/n$ for an $(n-1)$-fold Andreev reflection ($n = 2, 3, ...$) [39]. We observe additional subgap peaks, which shift in energy with tip approach. The set of peaks following $eV = \Delta_t - \epsilon$ arises from thermal excitations [18]. Interestingly, the contrast-enhanced plot of dI/dV spectra (Fig. 4a,b) shows two other sets of peaks, which follow the relation $eV = (\Delta_t + \epsilon)/n$ with $n = 2, 3$ [38] (Fig. 4d). They originate from the excitation of the YSR state by electron/holes that are Andreev reflected from the superconductor (Fig. 4c). Unlike conventional MARs, these processes reflect the asymmetry of the YSR states and might also be usable as fingerprints of the quantum phase transition.

Finally, when the tip is in contact with the molecule (as deduced from the flat $G - \Delta z$ curves in Fig. 2a and Fig. 3a), the Andreev reflections through the YSR states merge with the conventional MARs. In this contact regime, the coupling of the impurity to the tip and the surface start to compete which each another, leading to an effective coupling of the two electrodes. As a result, an applied bias drives the junction out of equilibrium so that signatures of local excitations can be no longer detected in spectroscopic measurements [40].

In conclusion, we have realized a magnetic-impurity junction whose exchange coupling can be precisely, continuously, and reversibly tuned through mechanical forces exerted by an STM tip. Varying the junction conductance by almost three orders of magnitude enabled us to access various transport regimes. We have employed this setup for a detailed investigation of the quantum phase transition between the screened-spin and free-spin ground states. We confirm the first-order nature of the transition in that the spectral weights of the single-particle addition spectrum change abruptly at the transition. We do not observe the predicted discontinuous jumps in the YSR energy and the local order parameter. Our analytical estimates show that the expected jumps in YSR energies are orders of magnitude smaller than the energy resolution even at mK temperatures. Finally, we emphasize that our results highlight a method for unambiguously determining the nature of the ground state by varying the exchange coupling.

We thank S. Loth for discussions. Financial support by Deutsche Forschungsgemeinschaft through grants HE7368/2 and CRC 183, and by the European Research Council through the consolidator grant "NanoSpin" is gratefully acknowledged. FvO performed part of this work at the Aspen Center for Physics supported by NSF grant PHY-1607611.

[1] L. Yu, Acta Phys. Sin. **21**, 75 (1965).
[2] H. Shiba, Prog. Theor. Phys. **40**, 435 (1968).
[3] A. I. Rusinov, Sov. J. Exp. Theor. Phys. **29**, 1101 (1969).
[4] A. Sakurai, Prog. Theor. Phys. **44**, 1472 (1970).
[5] T. Matsuura, Prog. Theor. Phys. **57**, 1823 (1977).
[6] O. Sakai, Y. Shimizu, H. Shiba, and K. Satori, J. Phys. Soc. Jpn. **62**, 3181 (1993).
[7] A. V. Balatsky, I. Vekhter, and J. X. Zhu, Rev. Mod. Phys. **78**, 373 (2006).
[8] B. W. Heinrich, J. I. Pascual, and K. J. Franke, Prog. Surf. Sci. **93**, 1 (2018).
[9] M. I. Salkola, A. V. Balatsky, and J. R. Schrieffer, Phys. Rev. B **55**, 12648 (1997).
[10] M. E. Flatté and J. M. Byers, Phys. Rev. B **56**, 11213 (1997).
[11] T. Meng, J. Klinovaja, S. Hoffman, P. Simon, and D. Loss, Phys. Rev. B **92**, 064503 (2015).
[12] R. Maurand, T. Meng, E. Bonet, S. Florens, L. Marty, and W. Wernsdorfer, Phys. Rev. X **2**, 011009 (2012).
[13] R. Delagrange, D. J. Luitz, R. Weil, A. Kasumov, V. Meden, H. Bouchiat, and R. Deblock, Phys. Rev. B **91**, 241401 (2015).
[14] R. Delagrange, R. Weil, A. Kasumov, M. Ferrier, H. Bouchiat, and R. Deblock, Phys. Rev. B **93**, 195437 (2016).
[15] R. S. Deacon, Y. Tanaka, A. Oiwa, R. Sakano, K. Yoshida, K. Shibata, K. Hirakawa, and S. Tarucha, Phys. Rev. Lett. **104**, 076805 (2010).
[16] E. J. Lee, X. Jiang, M. Houzet, R. Aguado, C. M. Lieber, and S. De Franceschi, Nat. Nanotechnol. **9**, 79 (2014).
[17] E. J. H. Lee, X. Jiang, R. **Z**itko, R. Aguado, C. M. Lieber, and S. De Franceschi, Phys. Rev. B **95**, 180502 (2017).
[18] M. Ruby, F. Pientka, Y. Peng, F. von Oppen, B. W. Heinrich, and K. J. Franke, Phys. Rev. Lett. **115**, 087001 (2015).
[19] A. Yazdani, B. A. Jones, C. P. Lutz, M. F. Crommie, and D. M. Eigler, Science **275**, 1767 (1997).
[20] S.-H. Ji, T. Zhang, Y.-S. Fu, X. Chen, X.-C. Ma, J. Li, W.-H. Duan, J.-F. Jia, and Q.-K. Xue, Phys. Rev. Lett. **100**, 226801 (2008).
[21] K. J. Franke, G. Schulze, and J. I. Pascual, Science **332**, 940 (2011).
[22] G. C. Ménard, S. Guissart, C. Brun, S. Pons, V. S. Stolyarov, F. Debontridder, M. V. Leclerc, E. Janod, L. Cario, D. Roditchev, P. Simon, and T. Cren, Nat. Phys. **11**, 1013 (2015).
[23] M. Ruby, Y. Peng, F. von Oppen, B. W. Heinrich, and K. J. Franke, Phys. Rev. Lett. **117**, 186801 (2016).
[24] D. J. Choi, C. Rubio-Verdú, J. De Bruijckere, M. M. Ugeda, N. Lorente, and J. I. Pascual, Nat. Commun. **8**, 15175 (2017).
[25] L. Cornils, A. Kamlapure, L. Zhou, S. Pradhan, A. A. Khajetoorians, J. Fransson, J. Wiebe, and R. Wiesendanger, Phys. Rev. Lett. **119**, 197002 (2017).
[26] M. Ruby, F. Pientka, Y. Peng, F. von Oppen, B. W. Heinrich, and K. J. Franke, Phys. Rev. Lett. **115**, 197204 (2015).
[27] N. Hatter, B. W. Heinrich, M. Ruby, J. I. Pascual, and K. J. Franke, Nat. Commun. **6**, 8988 (2015).
[28] N. Hatter, B. W. Heinrich, D. Rolf, and K. J. Franke, Nat. Commun. **8**, 2016 (2017).
[29] B. W. Heinrich, L. Braun, J. I. Pascual, and K. J. Franke, Nano Lett. **15**, 4024 (2015).
[30] R. Hiraoka, E. Minamitami, R. Arafune, N. Tsukuhara, S. Watanabe, M. Kawai, and N. Takagi, Nat. Commun. **8**, 16012 (2017).
[31] J. Brand, S. Gozdzik, N. Néel, J. L. Lado, J. Fernández-Rossier, and J. Kröger, Phys. Rev. B **97**, 195429 (2018).
[32] See supplementary material (which includes Ref.[41–43]) for considerations of the relevant parameters, a theoretical description of the change in local order parameter and YSR states, including an analytical estimation, experimental evidence for the absence of a Cl ligand on FeP, and additional experimental data FeP molecules in different environment.
[33] M. Ruby, B. W. Heinrich, J. I. Pascual, and K. J. Franke, Phys. Rev. Lett. **114**, 157001 (2015).
[34] J. Bauer, J. I. Pascual, and K. J. Franke, Phys. Rev. B **87**, 075125 (2013).
[35] M. E. Ali, B. Sanyal, and P. M. Oppeneer, J. Phys. Chem. B **116**, 5849 (2012).
[36] S. Bhandary, M. Schüler, P. Thunström, I. Di Marco, B. Brena, O. Eriksson, T. Wehling, and B. Sanyal, Phys. Rev. B **93**, 155158 (2016).
[37] C. Rubio-Verdú, A. Sarasola, D.-J. Choi, Z. Majzik, R. Ebeling, M. R. Calvo, M. M. Ugeda, A. Garcia-Lekue, D. Sánchez-Portal, and J. I. Pascual, Commun. Phys. **1**, 15 (2018).
[38] M. T. Randeria, B. E. Feldman, I. K. Drozdov, and A. Yazdani, Phys. Rev. B **93**, 161115 (2016).
[39] M. Ternes, W. D. Schneider, J. C. Cuevas, C. P. Lutz, C. F. Hirjibehedin, and A. J. Heinrich, Phys. Rev. B **74**, 132501 (2006).
[40] B. M. Andersen, K. Flensberg, V. Koerting, and

J. Paaske, Phys. Rev. Lett. **107**, 256802 (2011).
[41] B. W. Heinrich, G. Ahmadi, V. L. Müller, L. Braun, J. I. Pascual, and K. J. Franke, Nano Lett. **13**, 4840 (2013).
[42] B. W. Heinrich, L. Braun, J. I. Pascual, and K. J. Franke, Nat. Phys. **9**, 765 (2013).
[43] F. Pientka, L. I. Glazman, and F. von Oppen, Phys. Rev. B **88**, 155420 (2013).